Efficient density-functional theory integrations by locally augmented radial grids

Jürgen Gräfenstein[a)]
Department of Chemistry, Göteborg University, S-412 96 Göteborg, Sweden

Dieter Cremer
Department of Chemistry and Department of Physics, University of the Pacific, 3601 Pacific Ave., Stockton, California 95211-0110, USA

(Received 26 June 2007; accepted 11 September 2007; published online 30 October 2007)

Standard density-functional theory integration grids have proven insufficient for the meta generalized gradient approximation description of weakly bound complexes [E. R. Johnson *et al.*, Chem. Phys. Lett. **394**, 334 (2004)]. This is caused by an insufficient radial resolution in the valence region of frequently used standard grids. We present an algorithm for the construction of locally augmented radial grids, which allows us to enhance the resolution of a given radial grid in a specified region, thus increasing the accuracy of the standard grid in a cost-efficient way. Test calculations with the Van Voorhis-Scuseria exchange and correlation functional for the Ar dimer confirm that a suitably constructed, locally augmented radial grid with 100 points provides an accuracy competitive to that of a 250-point nonaugmented grid. Time savings and possible applications for locally augmented radial grids are discussed. © *2007 American Institute of Physics*. [DOI: 10.1063/1.2794038]

I. INTRODUCTION

Density-functional theory[1] (DFT) calculations employing meta generalized gradient approximation (m-GGA) exchange and correlation[2] (XC) functionals are a prospective approach for an efficient computational description of a wide class of chemical problems such as weakly bonded systems. In DFT calculations, the XC terms are usually calculated by numerical integration employing discrete integration grids. In a recent study,[3] Johnson *et al.* investigated the description of several van der Waals complexes with a number of DFT methods. It turned out that for m-GGA functionals, the standard integration grids used in modern quantum chemistry packages are insufficient for an accurate calculation of the XC terms, which resulted among others in qualitatively incorrect dissociation curves for the Ar dimer. A correct description required integration grids containing 250 points for radial integration, as compared to 75 or 99 points used in standard grids, which leads to a substantial increase in computation time.

The numerical integration of the XC term integration is usually performed atom by atom in spherical coordinates centered at the nuclei, with the three-dimensional integration being broken down into a one-dimensional radial and a two-dimensional angular integration. A variety of standard grids are available for the radial[4–11] and angular[12] integrations around a given atomic nucleus. The dimensioning of these grids is a trade-off between numerical accuracy and computational efficiency. The elaborate adaptive integration schemes[11,13] start with coarse grids and increase the grid resolution stepwise until the required accuracy is reached.

The accurate description of weakly bound complexes requires a numerically accurate description of the valence region (i.e., the region outside the Slater atomic radius[14]). Standard integration grids[4–11] are constructed in a way that they provide a high numerical accuracy close to the nucleus and a continuously decreasing one with increasing radius. If the accuracy of such a grid is enlarged by adding more grid points, the resolution of the grid will be uniformly increased over the whole range of radii. In addition to the required additional grid points in the outer valence region, one generates unnecessary additional grid points in the core region as well as far away from the atom, which increases the numerical cost of the calculations. It would therefore be an attractive alternative to refine the integration grid just in those regions where a higher numerical accuracy is required and leave it essentially unchanged elsewhere. In the present paper, we suggest an algorithm for the construction of such locally augmented radial integration grids. The method allows to increase the resolution of any standard integration grid in a given range by a specified factor. The construction of such locally augmented integration grids can be seen as a counterpart to the construction of augmented basis sets, where given standard basis sets are extended specifically in those regions where an increased numerical accuracy is required (e.g., by adding diffuse functions).

The present work is organized as follows. In Sec. II, we present our algorithm for a local augmentation of radial integration grids whereas in Sec. III, the computational procedures used are described. In Sec. IV, the performance of locally augmented radial grids is tested for one of the cases that was found especially problematic in Ref. 3, viz., the description of the Ar dimer with the Van Voorhis-Scuseria

[a)]Electronic mail: jurgen.grafenstein@chem.gu.se

exchange and correlation (VSXC) functional [2*b*]. Section V presents conclusions and discusses other possible applications of locally augmented radial grids.

II. THEORY

In numerical integrations, the integral over the molecular volume is usually partitioned into a sum of atomic integrals. A number of partitioning schemes are available for this purpose, of which the schemes by Becke[4] and Stratmann *et al.*[15] are used most widely today. Thus, we seek a quadrature formula for the atomic integral at atom *A*,

$$I_A = \int d^3 r f_A(\mathbf{r}), \tag{1}$$

where the nucleus of *A* is located at $\mathbf{r}=0$ and $f(\mathbf{r})$ is an atomic function, which may take large values and oscillate rapidly for small $r(r=|\mathbf{r}|)$ whereas it takes small values and decays relatively smoothly for $r\to\infty$. [For brevity, we drop the index *A* in Eq. (2) and in the following.] In spherical coordinates, Eq. (1) takes the form

$$I = \int_0^\infty dr r^2 \bar{f}(r), \tag{2a}$$

$$\bar{f}(r) = \int_0^{2\pi} d\varphi \int_0^\pi d\theta \sin\theta f(r,\theta,\varphi). \tag{2b}$$

In production calculations, the angular integration in Eq. (2b) is performed most efficiently by Lebedev quadrature,[12] which treats the φ and θ integrations in one step. For benchmark calculations, if the required accuracy exceeds that of the largest available Lebedev grids, the φ and θ integrations have to be performed separately, see, e.g., Ref. 8.

The accuracy of the angular integration is determined by the size of the integration grid used. There are two important ways of improving the efficiency of the angular integration: (i) One way is by varying the size of the angular grid in dependence on *r* using large angular grids in the valence region and smaller grids in the core and possibly the outer valence region. By this *angular pruning*, one improves the balance between radial and angular resolutions and avoids costly calculations in regions where the integrand is nearly spherically symmetric. (ii) A more advanced approach is the *adaptive grid generation*, where, for each *r*, one starts with a coarse angular grid and increases the size of the angular grid until the required accuracy is reached. Such adaptive schemes have been suggested by Köster and co-workers[11] as well as Pérez-Jordá *et al.*[13] While Köster and co-workers[11] used a fixed radial grid, in the scheme by Pérez-Jordá *et al.*[13] the size of the radial grid is adapted as well, i.e., one starts with a coarse radial grid, which is refined until the required accuracy is reached.

For the construction of the radial integration grid, a variety of algorithms have been suggested in the literature. All of them can be decomposed into two steps: (i) The integration interval $[0,\infty]$ is transformed to a finite interval of the dimensionless variable *t* by a suitable variable transformation $R(t)$. The integral *I* takes then the form

$$I = \int_a^b dt R'(t) R^2(t) \bar{f}[R(t)]. \tag{3}$$

(ii) In the second step, the integral in Eq. (3) is calculated approximately by a numerical quadrature. Generally, a numerical quadrature amounts to the approximation

$$\int_a^b dx F(x) \approx \sum_{k=1}^N \omega_k^N F(\xi_k^N), \tag{4}$$

where *F* is the function to be integrated, *N* is the order of the quadrature scheme, and the values ξ_k^N and ω_k^N are the grid points and weights characteristic for the numerical quadrature scheme used. Combining Eqs. (3) and (4), one gets thus the approximate expression for *I*

$$I \approx \sum_{k=1}^N w_k^N \bar{f}(r_k^N), \tag{5a}$$

$$r_k^N = R(\xi_k^N), \tag{5b}$$

$$w_k^N = W(\xi_k^N)\omega_k^N, \tag{5c}$$

$$W(x) = R^2(x)R'(x), \tag{5d}$$

i.e., a sum of the values of *f* at the grid points r_k^N weighted with factors w_k^N. The augmentation procedure to be presented in this work is easiest to formulate for trapezoidal integration. Therefore, the description in the following will be based on the use of trapezoidal integration. The generalization to arbitrary numerical quadrature schemes will be given at the end of this section. For trapezoidal integration, which in the current context is equivalent to the Euler-MacLaurin integration formula, it is useful to choose the interval $[a,b]$ in Eq. (3) as $[0,N+1]$. Then, $\xi_k^N=k$, $\omega_k^N\equiv 1$, and Eqs. (5b) and (5c) take the simple forms

$$r_k^N = R(k), \tag{6a}$$

$$w_k^N = W(k), \tag{6b}$$

with $W(k)$ defined as in Eq. (5d).

For both steps (i) and (ii), a variety of algorithms are available. Expressions for $R(t)$ have been suggested, e.g., by Becke,[4] Murray *et al.*,[5] Treutler and Ahlrichs,[8] Mura and Knowles,[7] Gill and Chien,[9] and Lindh *et al.*[10] The function $R(t)$ has to be chosen in a way that a high resolution is provided in the core and, to a lesser extent, in the valence region of atom *A* to ensure an accurate integration but sparse outside the atomic region of *A* to allow an economical calculation. The resolution is controlled by the value of the derivative $R'(t)$: A small value of $R'(t)$ indicates that a given interval for *r* is mapped onto a large interval of *t*, which implies a high resolution; consequently, a large value of $R'(t)$ implies a low resolution. In summary, $R'(t)$ should be small where $R(t)$ is small and large where $R(t)$ is large.

The *m*th order Euler-MacLaurin (EM*m*) grid,[5,6] which is employed for the calculations in the present work, uses the transformation

$$R_{\mathrm{EM}m}(t) = R_0 \frac{t^m}{(N+1-t)^m}. \tag{7}$$

The parameter R_0 is a characteristic radius of atom A, e.g., the atomic radius according to the Slater rules.[9] Generally, any function R used in step (i) must contain at least one characteristic length to facilitate the transformation from r to the dimensionless variable t.

Eq. (7) implies

$$R'_{\mathrm{EM}m}(t) = (N+1)mR_0 \frac{t^{m-1}}{(N+1-t)^{m+1}}, \tag{8}$$

i.e., $R'_{\mathrm{EM}m}(t)$ increases from 0 ($t=0$, i.e., $r=0$) to ∞ ($t=N+1$, i.e., $r\to\infty$) as required. Following Murray *et al.*[5] and Gill *et al.*,[6] we use $m=2$.

For step (ii), various quadrature schemes are used as alternatives to the trapezoidal rule. Becke[4] and Treutler and Ahlrichs[8] used the Gauss-Chebyshev integration, whereas Gill and Chien[9] have developed a quadrature scheme adjusted to their choice of the transformation $R(t)$.

The overall resolution of a given radial grid can be easily increased by increasing N. However, if the resolution needs to be increased only in a limited interval of r or, equivalently, t values, increasing N globally would be uneconomical. Adaptive grid generators suggested by Pérez-Jordá *et al.*[13] and Köster and co-workers[11] let the size of the angular grid increase locally but do not provide any possibility of locally enhancing the radial resolution of the grid.

A possible way of increasing the local resolution of the grid might be to modify the parameter R_0 in Eq. (7) in a suitable way. However, as we shall see in Sec. IV, such a modification does not offer local resolution enhancement. One might try to find a suitably modified function R that accomplishes such an augmentation. Instead, we present a more straightforward procedure, which can be applied subsequently to any function $R(t)$. If the resolution of the grid is to be enhanced by a factor of Q in the interval $[N_1,N_2]$ for t $(0<N_1<N_2<N)$, i.e., the interval $[N_1,N_2]$ for t of the grid should be augmented by

$$\Delta N = \mathrm{int}[(Q-1)(N_2-N_1)] \tag{9a}$$

points, one will get a new grid with

$$\tilde{N} = N + \Delta N \tag{9b}$$

points. This new grid is generated by a coordinate transformation $t=T(\tau)$ that maps the interval $[0,N+1]$ for t on the interval $[0,\tilde{N}+1]$ for τ. The function T is chosen in a way that the intervals $[0,N_1]$, $[N_1,N_2]$, and $[N_2,N+1]$ for t are approximately mapped on the intervals $[0,N_1]$, $[N_1,N_2+\Delta N]$, and $[N_2+\Delta N,\tilde{N}+1]$ for τ in a way that $T'(\tau)\approx 1$ in the first and third of the intervals and $T'(\tau)\approx 1/Q$ in the second one. Apart from this, $T'(\tau)$ has to be continuous in the integration domain. A suitable expression for $T'(\tau)$ is

$$T'(\tau) = 1 - D\left[\frac{1}{e^{\alpha(N_1-\tau)}+1} - \frac{1}{e^{\alpha(\tilde{N}_2-\tau)+1}}\right], \tag{10a}$$

$$\tilde{N}_2 = N_2 + \Delta N. \tag{10b}$$

Here, the parameter α ($\alpha>0$) can be chosen freely. Large α values provide an abrupt transition and small α values a smooth transition between nonaugmented and augmented regions. The parameter D is approximately $D\approx 1-1/Q$ where the exact value is stipulated by the boundary conditions for $T(\tau)$ [see Eq. (12b) below]. Integration of Eqs. (10a) and (10b) gives

$$T(\tau) = \tau - \frac{D}{\alpha}\log\left[C\frac{e^{\alpha(N_1-\tau)}+1}{e^{\alpha(\tilde{N}_2-\tau)}+1}\right]. \tag{11}$$

The constants C and D follow from the boundary conditions as

$$C = \frac{e^{\alpha\tilde{N}_2}+1}{e^{\alpha N_1}+1}, \tag{12a}$$

$$D = \frac{\Delta N\alpha}{\log\dfrac{[e^{\alpha(N_1-\tilde{N}-1)}+1](e^{\alpha\tilde{N}_2}+1)}{[e^{\alpha(\tilde{N}_2-\tilde{N}-1)}+1](e^{\alpha N_1}+1)}}. \tag{12b}$$

Then, the integral in Eq. (3) can be written as

$$I = \int_0^{\tilde{N}+1} d\tau T'(\tau)R'[T(\tau)]R^2[T(\tau)]\bar{f}\{R[T(\tau)]\}, \tag{13}$$

which again can be calculated approximately by the trapezoidal rule

$$I \approx \sum_{k=1}^{\tilde{N}} \tilde{w}_k^{\tilde{N}} \bar{f}(\tilde{r}_k^{\tilde{N}}), \tag{14a}$$

$$\tilde{w}_k^{\tilde{N}} = T'(k)W(t_k), \tag{14b}$$

$$\tilde{r}_k^{\tilde{N}} = R(t_k), \tag{14c}$$

$$t_k = T(k). \tag{14d}$$

Equations (5d), (9a), (9b), (11), (12a), (12b), and (14a)–(14d) provide a computational scheme for the construction and use of a *locally augmented radial grid* starting from the radial grid given by the transformation function $R(t)$.

There are situations where the augmentation interval should stretch to the position of the nucleus (i.e., $N_1=0$) or to infinity (i.e., $N_2=N+1$). In these cases, the Fermi function containing $\tilde{N}_2$ or N_1, respectively, should not be present in $T'(\tau)$; instead, $T'(\tau)$ should take the form

$$T'(\tau) = 1 - \frac{d}{e^{\mp\alpha(N_X-\tau)}+1}, \tag{15}$$

with a suitably chosen d, the upper (lower) signs being applicable to $N_1=0$ ($N_2=N$), and

$$N_X = \begin{cases} \tilde{N}_2 & \text{for } N_1 = 0 \\ N_1 & \text{for } N_2 = N. \end{cases} \tag{16}$$

Equation (15) leads to the following modified form of $T(\tau)$:

$$T(\tau) = (1-d)\tau \pm \frac{d}{\alpha}\log\{c[e^{\mp\alpha(N_x-\tau)}+1]\}, \tag{17}$$

with the constants

$$c = \frac{1}{e^{\mp\alpha N_x}+1}, \tag{18a}$$

$$d = \frac{1}{1 \mp \frac{1}{\alpha(\tilde{N}+1)}\log\{c[e^{\mp\alpha(N_x-\tilde{N}-1)}+1]\}}. \tag{18b}$$

Equations (5d), (9a), (9b), (14a)–(14d), (17), (18a), and (18b) form the set of working equations for this case.

Finally we give the counterpart to Eqs. (14a)–(14d) for arbitrary quadrature schemes. In the literature, the ξ_k^N and ω_k^N values for quadrature schemes are usually given for a fixed (i.e., N-independent) interval $[a,b]$, e.g., $[0,1]$ or $[-1,1]$. Therefore, we assume here that a and b are independent of N. To find the counterpart to Eqs. (14b)–(14d) for this case, one has to subject the variables t and τ to appropriate linear transformations, which results in the set of equations

$$\tilde{w}_k^{\tilde{N}} = \frac{\tilde{N}+1}{N+1}T'(\tau_k)W(t_k)\omega_k^{\tilde{N}}, \tag{19a}$$

$$\tilde{r}_k^{\tilde{N}} = R(t_k), \tag{19b}$$

$$t_k = a + \frac{b-a}{N+1}T(\tau_k), \tag{19c}$$

$$\tau_k = \frac{\tilde{N}+1}{b-a}(\xi_k^{\tilde{N}} - a). \tag{19d}$$

These equations replace Eqs. (14b)–(14d) and are to be used together with Eq. (14a).

III. COMPUTATIONAL PROCEDURES AND CONVENTIONS

The local augmentation according to Eqs. (11), (12a), (12b), and (14a)–(14d) was implemented in the COLOGNE07 program package[16] for use with EMm/Lebedev (L) grids. We calculated dissociation curves, dissociation energies (D_e values), equilibrium bond lengths r_e, and harmonic vibration frequencies ω_e for the Ar dimer. To provide comparability with Ref. 3, we used the VSXC functional $[2b]$ and the 6-31G(d) basis set.[17] This basis set is too small to provide reliable results for the Ar dimer but sufficient to assess the stability of the numerical DFT integration $[3b,c]$. Therefore, we verified our final findings by calculations with Dunning's aug-cc-pVTZ basis set.[18] For the XC integrations, we used an augmented EM2/L grid, which is described in detail in Sec. IV, and, for reference calculations, standard (75,302), (99,590), (150,590), and (250,590) EM2/L grids. For R_0, a value of 0.70 Å was used.[6]

In production calculations, angular pruning is used to increase numerical efficiency.[5,6] In the present work, we proceed in two steps. In the first step, we use unpruned integration grids to get a clear account of the radial grids. In the second step, we repeat the calculations with the (250,590) and $(100_{75},590)$ grids applying angular pruning for the purpose of testing which impact pruning has on the numerical accuracy and the computational cost of calculations employing locally augmented grids. Reference 6 suggests a pruning scheme for Ar where Lebedev grids of sizes of 6, 38, 86, 194, and 86, respectively, were used in the r intervals $[0,0.1R_0]$, $[0.1R_0,0.4R_0]$, $[0.4R_0,0.8R_0]$, $[0.8R_0,2.5R_0]$, and $[2.5R_0,\infty]$, respectively. We modified this scheme in the way that we kept the radial intervals but replaced the 194-point grid by a 590-point grid and increased the grid size for the other intervals proportionally. This recipe led to grid sizes of 18, 146, 302, 590, and 302 points, respectively.

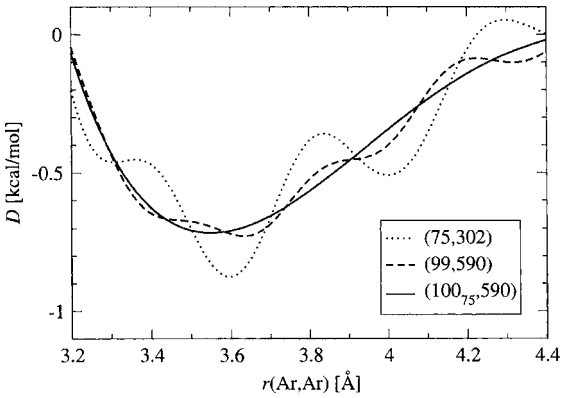

FIG. 1. Dissociation curve for the Ar dimer calculated with the VSXC functional $[2b]$ and the 6-31G(d,p) (Ref. 17) basis set using different standard and augmented DFT integration grids. See Sec. IV for a detailed description of the grids.

An integration grid of insufficient size may give accurate results by an accidental compensation of errors. In order to detect such cases, for each N-point radial grid considered, we repeated the geometry optimization with the corresponding $N+1$, $N+2$, $N+3$, and $N+4$ point grids. For instance, we repeated the calculation with (251,590), (252,590), (253,590), and (254,590) grids to assess the quality of the (250,590) grid. The ranges (i.e., difference between maximum and minimum values) ΔD_e, Δr_e, and $\Delta\omega_e$ of the D_e, r_e, and ω_e values obtained for such a series of five grids are used to assess the reliability of the result for the N-point grid.

IV. RESULTS AND DISCUSSION

First, we calculated the dissociation curve of the Ar dimer to get an initial assessment of the performance of the locally augmented EM2/L grid. Figure 1 shows the dissociation curve of the Ar dimer for r(Ar,Ar) varying from 3.2 to 4.5 Å as calculated with different standard and aug-EM2/L grids. For a standard (75,302) grid, the curve shows substantial oscillations and multiple minima, in agreement with the findings in Ref. 3. (Note that pruned grids are used in Ref. 3; therefore, the dissociation curve in the present work differs from that in Ref. 3.) For a (99,590) EM2/L grid, the oscillations are less pronounced but still clearly visible. In Ref. 3, it had been shown that a (250,590) EM2/L grid provides a correct dissociation curve without spurious oscillations. We therefore constructed an augmented (aug-)EM2/L

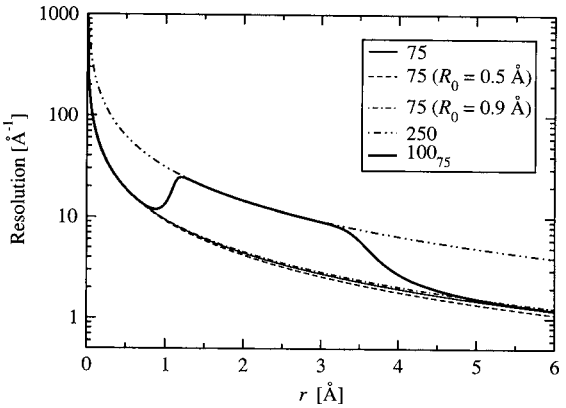

FIG. 2. Radial resolution vs distance from the nucleus for different augmented and nonaugmented EM2 radial grids for the Ar atom. For the augmented 100_{75} grid, $N_1=42$, $N_2=53$, and $\alpha=50/(75+1)\approx 0.6579$ (see Sec. II for details). Unless otherwise stated, $R_0=0.7$ Å for all grids.

grid that has the same radial resolution as the (250,590) grid in the region between the two Ar atoms and a radial resolution comparable to the standard (75,302) grid in the core region as well as far away from the atoms. For this purpose, we chose $Q=250/75=10/3$. The interval boundaries N_1 and N_2 were chosen to be 56% and 70% of 75+1, respectively, i.e., after rounding, $N_1=38$ and $N_2=66$. This choice implies that the augmentation region ranges from $r=1.62R_0=1.13$ Å to $r=5.44R_0=3.80$ Å [see Eq. (7)] and provides an aug-EM2 radial grid with $\tilde{N}=100$, i.e., a grid just 40% the size of the 250-point EM2 grid. We will in the following denote augmented radial grids by $\tilde{N}_N$, i.e., the present grid is denoted as 100_{75}. α was chosen as $50/(N+1)$ after a series of benchmark calculations.

Figure 1 reveals that the $(100_{75},590)$ aug-EM2/L grid provides a smooth dissociation curve without oscillations. A reference calculation showed that this dissociation curve agrees within 0.001 kcal/mol with the curve provided by the (250,590) grid (not shown in Fig. 1).

Figure 2 gives the radial resolution of the 100_{75} aug-EM2 grid as compared to a 75-point and a 250-point EM2 grid, respectively. Here, the radial resolution at r_k^N was determined as $2/(r_{k+1}^N-r_{k-1}^N)$, analogously for $\tilde{r}_k^{\tilde{N}}$. The graphs illustrate that the resolution of the 100_{75} aug-EM2 grid coincides with that of the 75-point EM2 grid for r up to ≈ 0.9 Å, increases continuously to that of the 250-point grid in a transition region up to ≈ 1.3 Å, coincides with that of the 250-point grid up to $r\approx 3.2$ Å, decreases continuously to that of the 75-point grid in a second transition region up to $r\approx 4.6$ Å, and coincides with that of the 75-point grid above that r value. It is noteworthy that the inner transition region covers a smaller r interval $(0.9,\ldots,1.3$ Å) than the outer one $(3.2,\ldots,4.6$ Å). This is related to the fact that the original transformation function $R(t)$ provides a radial resolution that decreases with r.

In Sec. II, we discussed the possibility of locally augmenting an EM2 grid by modifying R_0. For the purpose of testing this idea, we calculated the radial resolution of a 75-point EM2 grid for R_0 values of 0.5 and 0.9 Å. The results in Fig. 2 reveal that a variation of R_0 has only little impact on the radial resolution of an EM2 grid in the valence region, i.e., varying R_0 is no appropriate way of locally augmenting an EM2 radial grid.

TABLE I. Bond energy, equilibrium distance, and harmonic vibration frequency for the Ar dimer. Calculations done with the VSXC functional [2*b*] and the 6-31G(*d*,*p*) (Ref. 17) and aug-cc-pVTZ basis set (Ref. 18), respectively. D_e in kcal/mol, $r_e=r(\mathrm{Ar},\mathrm{Ar})$ in Å, and ω in cm^{-1}. ΔD_e, Δr_e, and $\Delta\omega_e$ indicate how much the calculated D_e, r_e, and ω_e values vary if the radial resolution of the grids is varied between N and $N+4$. See end of Sec. III for details. ΔD_e and Δr_e values below 0.001 kcal/mol and 0.001 Å, respectively, are not displayed. N_{tot} is the total number of grid points per atom.

Grid[a]	D_e	ΔD_e	r_e	Δr_e	ω_e	$\Delta\omega_e$	N_{tot}
6-31G(*d*,*p*) basis set							
(75,302)	0.876	0.130	3.596	0.246	165.26	13.27	22 650
(99,590)	0.728	0.045	3.631	0.157	100.33	27.03	58 410
(150,590)	0.716	0.002	3.551	0.008	66.84	9.31	88 500
(250,590)	0.715		3.550		62.26	0.01	147 500
$(100_{75},590)$	0.715		3.550		62.30	0.05	59 000
$(250,590)_P$	0.713		3.550		61.69	0.15	62 768
$(100_{75},590)_P$	0.713		3.550		61.71	0.13	29 420
aug-cc-pVTZ basis set							
(75,302)	0.940	0.136	3.598	0.256	172.88	25.16	22 650
$(250,590)_P$	0.755		3.575	0.001	54.95	0.18	62 768
$(100_{75},590)_P$	0.755		3.575	0.001	55.00	0.30	29 420

[a](N,L) denotes an unpruned N-point Euler-Maclaurin (Refs. 5 and 6)/L-point Lebedev (Ref. 12) gird; $(\tilde{N}_N,L)$, a grid with $\tilde{N}$ radial points generated by augmentation of an (N,L) Euler-Maclaurin/Lebedev grid. The subscript P indicates that the grid has been angularly pruned as described in Sec. III. See Sec. IV for details of the augmentation scheme.

A more stringent test of the performance of the aug-EM2 grid is given by the calculated bond energy, equilibrium bond distance and, above all, harmonic vibration frequencies of the Ar dimer. Table I lists calculated values for a variety of integration grids. The calculation with the (250,590) EM2/L grid yields $D_e=0.715$ kcal/mol, $r_e=3.550$ Å, and $\omega_e=62.26$ cm^{-1}. The test calculations with the (251,590) to (254,590) EM2/L grids give $\Delta D_e<10^{-3}$ kcal/mol, $\Delta r_e<10^{-3}$ Å, and $\Delta\omega_e=0.01$ cm^{-1}, respectively. These results confirm that the (250,590) EM2/L grid allows reliable DFT integrations in the present case, and the results calculated for this grid will be used as reference in the following.

The (75,302) grid, together with the 6-31G(*d*,*p*) basis set, yields a D_e value of 0.876 kcal/mol and $r_e=3.956$ Å with ΔD_e and Δr_e values of 0.13 kcal/mol and 0.246 Å, respectively. A comparison with the dissociation curve (Fig. 1) gives at hand that the geometry optimization converges to different local minima depending on details of the integration grid. The ω_e value of 165.3 cm^{-1} is too high by about 100 cm^{-1}, with $\Delta\omega_e=13.3$ cm^{-1}. The oscillations of the bond energy exaggerate the curvature of the dissociation curve, which accounts for the exaggeration of the ω_e values.

For the (99,590) grid, the same trends, though less pronounced, can be observed as for the (75,302) grid: ΔD_e and Δr_e are 0.05 kcal/mol and 0.16 Å, respectively, ω_e is 100.3 cm^{-1}, about 37 cm^{-1} above the reference value, and $\Delta\omega_e$ amounts to 27 cm^{-1}.

For a (150,590) EM2/L grid, one obtains D_e and r_e values that differ by just 0.002 kcal/mol and 0.001 Å, respec-

tively, from the reference value (Table I) and ΔD_e and Δr_e values of just 0.002 kcal/mol and 0.008 Å, whereas the vibration frequency (66.8 cm^{-1}) is 4 cm^{-1} larger than the reference value and $\Delta\omega_e=9.3$ cm^{-1}. The ω_e and $\Delta\omega_e$ values indicate that a standard EM2 radial grid requires about 250 rather than 150 points to provide an accurate description of the Ar dimer.

Our $(100_{75},590)$ aug-EM2/L grid reproduces the reference values for D_e and r_e by less than 10^{-3} kcal/mol and 10^{-3} Å, respectively, and ω by 0.04 cm^{-1}. For the purpose of determining ΔD_e, Δr_e, and $\Delta\omega_e$, we constructed a series of four aug-EM2/L grids starting from the (76,590) to (79,590) EM2/L grids, respectively, in the same way as we constructed the $(100_{75},590)$ aug-EM2/L grid. We obtained $(99_{76},590)$, $(102_{77},590)$, $(103_{78},590)$, and $(106_{79},590)$ aug-EM2/L grids. The calculations with these grids yielded $\Delta D_e<10^{-3}$ kcal/mol, $\Delta r_e<10^{-3}$ Å, and $\Delta\omega_e=0.05$ cm^{-1}. These results indicate that, for the problem investigated, the $(100_{75},590)$ aug-EM2/L grid provides the same accuracy as the (250,590) EM2/L grid and is clearly superior to the (larger) standard (150,590) EM2/L grid.

The calculations with the pruned (250,590) grid (pruning is denoted with the subscript P in the following, see Table I) show that pruning gives rise to a decrease of D_e by 2 cal/mol. The value for r_e changes by just 0.001 Å. ΔD_e and Δr_e are below 10^{-3} kcal/mol and 10^{-3} Å, respectively. The ω_e value is decreased by about 0.5 cm^{-1}; also, $\Delta\omega_e$ increases to 0.15 cm^{-1} as compared to 0.01 cm^{-1} for the (250,590) grid. The changes in D_e and ω_e and the increase in $\Delta\omega_e$, although noticeable, are insignificant in practical applications. The $(100_{75},590)_P$ grid yields the same D_e and r_e values as the $(250,590)_P$ grid and an ω_e value just 0.02 cm^{-1} lower, ΔD_e and Δr_e values below 10^{-3} kcal/mol and 10^{-3} Å, respectively, and a $\Delta\omega_e$ of 0.13 cm^{-1}. Thus, the 100_{75} radial grid provides the same accuracy as the 250-point radial grid, regardless whether angular pruning is applied or not.

It is instructive to discuss the numerical efficiency of the aug-EM2 radial grids in connection with angular pruning. The augmentation adds radial grid points just in the region where the angular resolution is highest. In this way, the reduction of the radial grid size compared to a fine standard EM2 grid is concentrated on regions where the angular resolution is lower. Thus, one might suspect that the computational gain available by aug-EM2 grids is small. The rightmost column of Table I shows the sizes of the different grids used. One finds that the $(100_{75},590)_P$ aug-EM2/L grid is just 47% the size of the $(250,590)_P$ EM2/L grid. The savings in CPU time amount to 40% for the frequency calculation and 35% for a complete calculation comprising optimization and frequency calculation. We remark that the $(100_{75},590)_P$ aug-EM2/L grid is just 55% larger than a $(75,590)_P$ EM2/L grid generated with our pruning scheme would be. In conclusion, pruned aug-EM2/L grids provide a substantial computational gain relative to pruned fine standard-EM2/L grids. One has to keep in mind in this connection that the computational cost for the extra coordinate transformation is negligible compared to the savings in the numerical integration.

The calculations with the (75,302), the $(250,590)_P$, and the $(100_{75},590)_P$ grids were repeated with the aug-cc-pVTZ basis set. The results in Table I indicate that the calculation with the (75,302) grids lead to the same problems as the corresponding calculations with the 6-31G(d,p) basis set. The results for the $(250,590)_P$ grid indicate an increase of D_e by 0.042 kcal/mol to a value of 0.755 kcal/mol, an increase of r_e by 0.025 Å to a value of 3.575 Å, and a decrease of ω_e by 7 cm^{-1} to a value of 55.0 cm^{-1}, as compared to the 6-31G(d,p) results. These significant changes corroborate that the 6-31G(d,p) basis set is insufficient for a description of weakly bound complexes. Replacing the $(250,590)_P$ grid by the $(100_{75},590)_P$ grid leaves the D_e and r_e as well as ΔD_e and Δr_e values unchanged, increases ω_e by 0.05 cm^{-1}, and increases $\Delta\omega_e$ slightly from 0.18 to 0.30 cm^{-1}. These results indicate that the aug-EM2 radial grids work properly with a large basis set containing diffuse functions.

V. CONCLUSIONS

We have presented an algorithm that allows to augment radial integration grids locally in regions where an increased numerical accuracy is required. The algorithm can be applied to any existing radial grid and provides an economical alternative to an overall refinement of the existing grid type by increasing the total number of grid points. It is easy to implement and causes no substantial extra computational cost in the grid generation. The new algorithm was tested for the treatment of the Ar dimer with the VSXC functional [4*b*]. A previous investigation[3] had demonstrated that the standard integration grids used in modern quantum-chemical program packages provide a qualitatively incorrect dissociation curve in this case. In this work, we show that a properly augmented EM2 radial grid with 100 radial points provides a stable and accurate description of this problem, whereas a nonaugmented EM2 grid requires 250 radial points for a stable description,[3] which allows savings in CPU time of 35%–40%. It was shown that the aug-EM2 radial grids provide accurate results in connection with angular pruning and work properly for extended basis sets containing diffuse functions. This result is encouraging and indicates that standard integration grids that are augmented in the outer valence region provide an interesting alternative to large standard grids for the treatment of weakly bound complexes with m-GGA methods.

A possible direction for future work is the combination of locally augmented radial grids with adaptive grid generators[13,11] to optimize the computational cost.

There are more potential applications for locally augmented integration grids:

(1) Several problems, such as the determination of electric field gradients in heavy atoms and the determination of nuclear spin-spin coupling constants, require a high numerical resolution in the region very close to the nucleus. In these cases, a local augmentation of the integration grid close to the nucleus [i.e., case $N_1=0$ in Eqs. (15)–(18)] can provide this accuracy in an efficient way. By choosing a relatively small value of α in Eq. (17), it is possible to realize an enhancement of the resolution that increases continuously as one ap-

proaches the nucleus position. Such an augmentation of the integration grid can be seen as a complement to the augmentation of the basis set with compact functions as suggested, e.g., in Ref. 19.

(2) Some years ago, numerical basis sets have been introduced as an alternative to standard Gaussian- or Slater-type basis sets (see, e.g., Ref. 20). For numerical basis sets, the values of the basis functions are given on a discrete grid of points, and all energy contributions, etc., are calculated by numerical integrations. The proper choice of the grid is essential for a favorable ration between numerical expenses and accuracy, and locally augmented grids will be valuable if basis sets for special purposes are to be constructed.

ACKNOWLEDGMENTS

D.C. thanks the University of the Pacific for support of this work. Calculations were done on the computers of the National Supercomputer Center (NSC) in Linköping. The authors thank the NSC and the Swedish National Allocations Committee (SNAC) for a generous allotment of computer time.

[1] P. Hohenberg and W. Kohn, Phys. Rev. **136**, B864 (1964); W. Kohn and L. J. Sham, Phys. Rev. **140**, A1133 (1965).
[2] A. Becke, J. Chem. Phys. **104**, 1040 (1996); T. Van Voorhis and G. E. Scuseria, *ibid.* **109**, 400 (1998); J. M. Tao, J. P. Perdew, V. N. Staroverov, and G. E. Scuseria, Phys. Rev. Lett. **91**, 146401 (2003); J. P. Perdew, S. Kurth, A. Zupan, and P. Blaha, *ibid.* **82**, 2544 (1999); **82**, 5179(E) (1999).
[3] E. R. Johnson, R. A. Wolkow, and G. A. DiLabio, Chem. Phys. Lett. **394**, 334 (2004); R. J. Meier, *ibid.* **401**, 594 (2004); E. R. Johnson, R. A. Wolkow, and G. A. DiLabio, *ibid.* **401**, 595 (2004).
[4] A. Becke, J. Chem. Phys. **88**, 2547 (1988).
[5] C. W. Murray, N. C. Handy, and G. J. Laming, Mol. Phys. **78**, 997 (1993).
[6] P. M. W. Gill, B. G. Johnson, and J. A. Pople, Chem. Phys. Lett. **209**, 506 (1993).
[7] M. E. Mura and P. J. Knowles, J. Chem. Phys. **104**, 9848 (1996).
[8] O. Treutler and R. Ahlrichs, J. Chem. Phys. **102**, 346 (1995).
[9] P. M. W. Gill and S. H. Chien, J. Comput. Chem. **24**, 732 (2003).
[10] R. Lindh, P. Å. Malmqvist, and L. Gagliardi, Theor. Chem. Acc. **106**, 178 (2001); A. El-Sherbiny and R. A. Poirier, J. Comput. Chem. **25**, 1378 (2004).
[11] M. Krack and A. Köster, J. Chem. Phys. **108**, 3226 (1998); A. M. Köster, R. Flores-Moreno, and J. U. Reveles, *ibid.* **121**, 681 (2004).
[12] V. I. Lebedev, Zh. Vychisl. Mat. Mat. Fiz. **16**, 293 (1976); Dokl. Math. **45**, 587 (1992).
[13] J. M. Pérez-Jordá, A. Becke, and E. San-Fabián, J. Chem. Phys. **100**, 6520 (1994).
[14] J. C. Slater, Phys. Rev. **36**, 57 (1930).
[15] E. Stratmann, G. E. Scuseria, and M. J. Frisch, Chem. Phys. Lett. **257**, 213 (1996).
[16] E. Kraka, J. Gräfenstein, M. Filatov, H. Joo, D. Izotov, J. Gauss, Y. He, A. Wu, V. Polo, L. Olsson, Z. Konkoli, Z. He, and D. Cremer, COLOGNE07, University of the Pacific, Stockton, CA, 2007.
[17] M. M. Francl, W. J. Petro, W. J. Hehre, J. S. Binkley, M. S. Gordon, D. J. DeFrees, and J. A. Pople, J. Chem. Phys. **77**, 3654 (1982).
[18] D. E. Woon and T. H. Dunning, Jr., J. Chem. Phys. **98**, 1358 (1993).
[19] P. F. Provasi, G. A. Aucar, and S. P. A. Sauer, J. Chem. Phys. **112**, 6201 (2000); F. Jensen, J. Chem. Theory Comput. **2**, 1360 (2006).
[20] B. Delley, J. Chem. Phys. **92**, 508 (1990); J. M. Soler, E. Artacho, J. D. Gale, A. García, J. Junquera, P. Ordejón, and D. Sánchez-Portal, J. Phys. Condens. Matter **14**, 2745 (2002).